BBA - Bioenergetics 1860 (2019) 148090

Contents lists available at ScienceDirect

BBA - Bioenergetics

journal homepage: www.elsevier.com/locate/bbabio

Identification of assembly precursors to photosystems emitting fluorescence at 683 nm and 687 nm by cryogenic fluorescence microspectroscopy

Tomofumi Chiba, Yutaka Shibata*

Department of Chemistry, Graduate School of Science, Tohoku University, Aramaki Aza Aoba, Aoba-ku, Sendai 980-8578, Japan

ARTICLE INFO

Keywords:
C4 plant
Zea mays
Etiolated seedling
Singular-value decomposition
Photosystem I
Photosystem II

ABSTRACT

Photosystem I (PSI) and photosystem II (PSII) play key roles in photoinduced electron-transfer reaction in oxygenic photosynthesis. Assemblies of these PSs can be initiated by illumination of the etiolated seedlings (greening). The study aimed to identify specific fluorescence spectral components relevant to PSI and PSII assembly intermediates emerging in greening seedlings of *Zea mays*, a typical C4 plant. The different PSII contents between the bundle sheath (BS) and mesophyll (M) cells were utilized to spectrally isolate the precursors to PSI and PSII. The greening *Zea mays* leaf thin sections were observed with the cryogenic microscope combined with a spectrometer. With the aid of the singular-value decomposition analysis, we could identify four independent fluorescent species, SAS677, SAS685, SAS683, and SAS687, named after their fluorescence peak wavelengths. SAS677 and SAS685 are the dominant components after the 30-minute greening, and the distributions of these components showed no clear differences between M and BS cells, indicating immature cell differentiation in this developing stage. On the other hand, the 1-hour greening resulted in reduced distributions of SAS683 in BS cells leading us to assign this species to PSII precursors. The 2-hour greening induced the enrichment of SAS687 in BS cells suggesting its PSI relevance. Similarity in the peak wavelengths of SAS683 and the reported reaction center of PSII implied their connection. SAS687 showed an intense sub-band at around 740 nm, which can be assigned to the emission from the red chlorophylls specific to the mature PSI.

1. Introduction

The light reaction in the oxygenic photosynthesis is conducted by the two photoactive pigment-protein complexes called photosystem I (PSI) and photosystem II (PSII). They form huge super-complexes composed of multiple protein subunits and many cofactors, such as chlorophylls (Chl), carotenoids, quinones, and so on. In spite of the great successes in determining the atomic-level structures of these super-complexes by the X-ray crystallography [1,2] and more recently by the cryo-electron microscopy [3], it remains to be clarified how the delicate structures of these super-complexes are assembled in vivo. We have not yet well understood the mechanism by which various cofactors are inserted into their correct sites of the protein.

Light illumination of an etiolated angiosperm seedling initiates the assembly of photosynthetic apparatuses in etioplasts, the precursor to chloroplasts. Illumination of an etiolated seedling photoactivates the enzyme, protochlorophyllide oxidoreductase (POR), and then initiates the synthesis of Chl, leading to the accumulation of mature PSs (greening). Since a greening plant seedling is enriched in the assembly intermediates to PSs, it can serve as a model system for studying the assembly process of PSs. In fact, there is a long-standing history of study on the fluorescence components observed during the greening of angiosperm [4–10]. These studies have identified many spectral components in greening leaves, which, in principle, should be related to the assembly intermediates predicted in the currently proposed stepwise assembly models of PSs (for PSII [11–13], for PSI [14–16]). However, the link between each fluorescent component observed and the assembly intermediate remains ambiguous. This is partly due to the spectral overlaps of many species in the fluorescence components, the problem inherent in the observation of intact leaves.

In the present study, we focus on spectroscopic identifications of the fluorescent assembly intermediates to PSI and PSII, which accumulate during the greening of an etiolated plant leaf. To overcome the spectral-overlap problem, here we conduct cryogenic fluorescence

Abbreviations: PSI, photosystem I; PSII, photosystem II; BS, bundle sheathe; M, mesophyll; SAS, species-associated spectrum; Chl, chlorophyll; POR, protochlorophyllide-oxidoreductase; VB, vascular bundle; LED, light-emitting diode; CW, continuous wave; CCD, charge-coupled device; SVD, singular-value decomposition; LHCI, light-harvesting chlorophyll protein complex I; LHCII, light-harvesting chlorophyll protein complex II; RC, reaction center

* Corresponding author.
E-mail address: shibata@m.tohoku.ac.jp (Y. Shibata).

https://doi.org/10.1016/j.bbabio.2019.148090
Received 24 July 2019; Received in revised form 26 September 2019; Accepted 17 October 2019
Available online 31 October 2019

microspectroscopy using a C4 plant, *Zea* (*Z.*) *mays*. A leaf of a C4 plant contains two kinds of cells having significantly different PSII contents. Bundle sheath (BS) cells surrounding the vascular bundle (VB) specialize in the CO_2 fixation reaction and drastically reduce PSII contents to suppress the level of oxygen acting as an inhibitor of the CO_2 fixation. Ordinary oxygenic photosynthesis through the linear electron transfer proceeds exclusively in the mesophyll (M) cells located in the part farther from the VB. Greening C4 plants (*Z. mays*) were used in previous studies [6,9], in which BS and M cells were mechanically isolated and analyzed independently by fluorescence spectroscopy.

Here we use cryogenic fluorescence microspectroscopy to enable analysis of leaf cells that are more intact. Although we have already reported on a study using a similar approach [10], in that study, we could not obtain fluorescence spectra of all pixels in a fluorescence image due to instrumental limitation. In the present study, we could obtain full spectral information in an image by using a recently developed cryogenic microscope system [17] with a slight modification. Several independent spectral components could be derived by the aid of the singular-value decomposition (SVD) analysis of large quantities of spectral data. Spectral components enriched in BS cells could be assigned to precursors to PSI and those enriched in M cells to PSII precursors.

In the following sections, we will explain the methodology used in the present study. We will start the explanation of the experimental results of mature *Z. mays* leaves to demonstrate the potential of the present approach to distinguish BS and M cells. Then, we will discuss the results obtained with greening leaves illuminated for certain time periods up to 2 h. Finally, we will discuss the spectral features of the identified assembly precursors to PSI and PSII.

2. Materials and methods

2.1. Sample preparations

Maize (*Z. mays* L. *cv. Koshu*) seedlings were grown for 7 days on vermiculite and tap water in a growth chamber. Developed green seedlings were grown under a cycle of 23 °C with white light (5000 lx) for 14 h and 21 °C in darkness for 10 h. We call hereafter a leaf taken from thus grown seedlings "mature leaf". The etiolated seedlings were grown in darkness under the same temperature cycle. The greening of intact plants was performed by illumination with light from a light-emitting diode (LED) (LDA7L-G, Panasonic, Kadoma). This LED provides daylight-color light with a color temperature of 6500 K. The illumination intensity was adjusted to 11,000 lx (180 μmol m^{-2} s^{-1}) at the surface of the leaf to be used (the second leaf). Samples with three different illumination times, 30 min, 1 h, and 2 h, were prepared.

It typically took ca. 10 min to prepare thin sections from a leaf and set them in the sample holder and about 5 min to cool the sample below 0 °C. Thus, the second leaf was cut from a seedling about 15 min before the predetermined illumination time. Thin sections of a leaf were sliced near its center. For example, a 30-minute illuminated sample was prepared by cutting a leaf from a plant illuminated for 15 min, and thin sections were prepared by a razor under illumination with the same LED. Five to 10 leaf sections were dispersed in a pH 7.5, 50 mM HEPES-KOH buffer containing 330 mM D-sorbitol, 1 mM $MgCl_2$, 1 mM $MnCl_2$, 2 mM ethylenediaminetetraacetic acid (EDTA), and 5 mM sodium ascorbate. The suspension was sealed in a cavity between two 0.3-mm thick quartz cover slips with a diameter of 10 mm in a homemade sample holder and set in a flow-type cryostat (Microstat, Oxford Instruments, Eynsham). During cooling, the sample was kept illuminated with a white-light LED (MCWHL2-C3, Thorlabs, Newton) of the microscope providing cool white light. The light intensity at the sample position was adjusted to 11,000 lx (130 μmol m^{-2} s^{-1}). The sample temperature was measured by a chromel-gold/iron-alloy thermocouple.

2.2. Cryogenic microscope system

A homebuild cryogenic microscope system [17] was used. The system was specially designed to set a vacuum-compatible objective lens in the heat-insulating vacuum space. Since we needed observations with a wider field of view in the present study, we modified the system to set a dividing wall with a 0.5 mm-thick quartz window between the vacuum chamber and the space containing the objective lens to use a vacuum-incompatible objective lens (Plan Fluor ELWD 40×, numerical aperture 0.6, Nikon, Tokyo). The working distance of the objective lens is 2.7–3.7 mm depending on the thickness of the glass medium placed between the sample and the lens. In the present study, the thickness of the glass medium was 0.8 mm (0.3 mm for the cover slip and 0.5 mm for the window). The aberration due to the 0.8-mm-thick glass medium was diminished by the correction collar of the objective lens. Light from a CW diode laser (445 nm, Stradus 445, Vortran Laser Technology Inc., Sacramento) was used as the excitation light. The laser power for the measurements of leaf slices was ca. 2 μW at the sample position. The typical spatial resolution of the system was ca. 1.0 μm and 2.4 μm along the lateral and axial directions, respectively, estimated by a three-dimensional scanning of fluorescent beads with a diameter of 200 nm (F-8811, Thermo Fisher Scientific, Waltham). Fluorescence spectra of all pixels in an image were obtained by a liquid-nitrogen-cooled charge-coupled device (CCD) camera (PyLoN:100BR eXcelon, Princeton Instruments, Trenton) connected to a polychromator (MS2004i, SOL instruments, Minsk). The dwell time for each pixel was 50 ms. Due to the limitation of the memory size, it is impossible to scan an image with a number of pixels larger than 70 × 70. Accordingly, an image with 100 × 100 pixels was obtained by synthesizing 4 independently scanned quarter parts of the image composed of 50 × 50-pixels. Due to this process, images with 100 × 100 pixels in this article may contain unnaturally aligned dark pixels, which are the boundary between the original quarter images.

3. Results

Fig. 1A shows a 100 × 100-pixel fluorescence image around a vascular bundle (VB) of a mature *Z. mays* leaf section at 80 K. A VB is indicated by a circle drawn with a dotted line. 10,000 fluorescence spectra were obtained after one measurement of a fluorescence image. Spectra differ from each other, reflecting variable PSI/PSII ratios depending on the distance from the VB. From the large data set, we tried to identify a spectrum specific to each emitting species (hereafter called species-associated spectrum; SAS) contained in a sample with the aid of the singular-value decomposition (SVD) analysis [18,19]. The SVD process decomposes a data matrix, whose *j*-th column corresponds to the emission spectrum at the *j*-th pixel, into a product of three matrices, *U*, *S*, and *V*. In the *S* matrix, only the diagonal components have non-zero positive values, λ_i, called singular values (SVs). The *i*-th column of *U* is called the basis spectrum associated with λ_i, reflecting the characteristic variations in the total series of the obtained data. The number N_c of SVs whose amplitude is beyond the noise level of the measurement gives the estimation of that of independent components that can be identified from the measurement. Thus, any emission spectra contained in the data matrix can be well approximated by the linear combination of the first to N_c-th basis spectra.

Solid lines in Fig. 2B show the basis spectra associated with the largest three SVs obtained by the SVD analysis of the data shown in Fig. 1. To reduce the data size of fluorescence spectra, we analyzed only spectral data in a range of 636–782 nm. The basis spectra shown in Fig. 2B are multiplied by the associated SVs. The six largest SVs are plotted in the Fig. 2 inset. After the third one, SVs have only negligible amplitudes, indicating that linear combinations of the three basis spectra in Fig. 2B can well approximate any of the 10,000 fluorescence spectra in the image.

The basis spectra associated with the three largest singular values

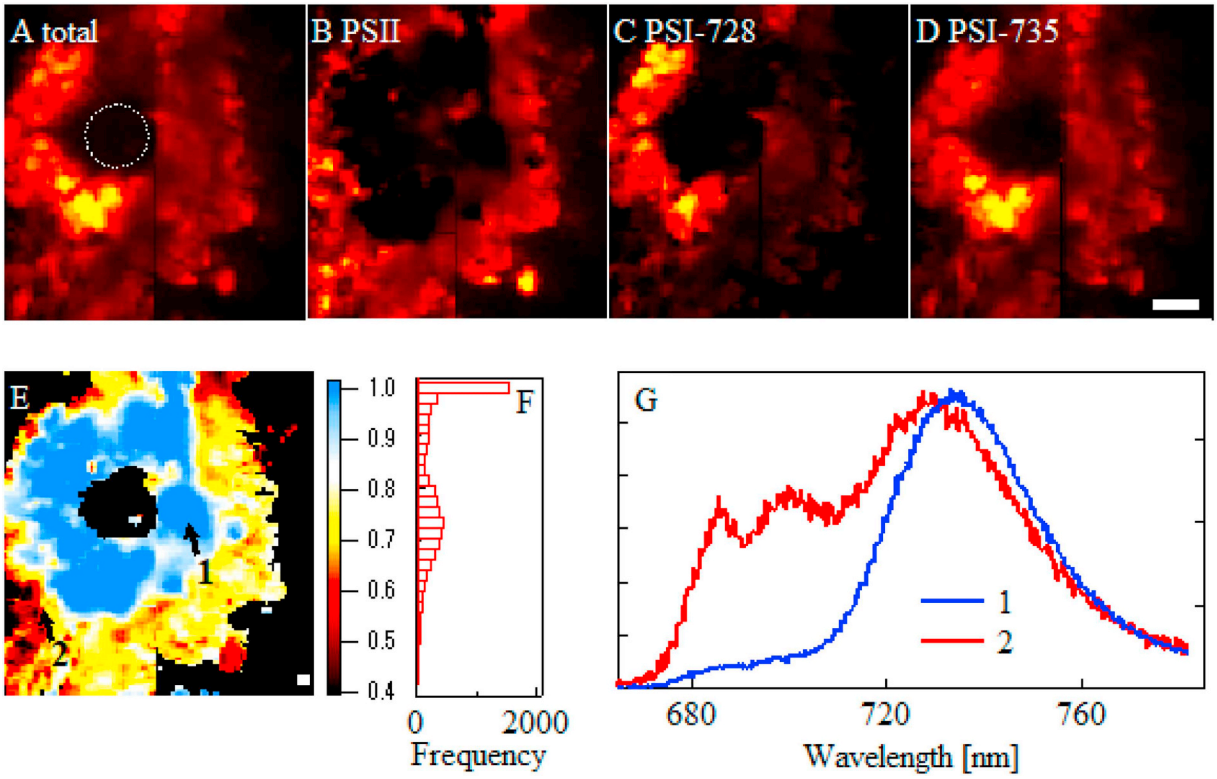

Fig. 1. (A) A fluorescence image around a vascular bundle of a mature *Z. mays* leaf section observed at 80 K. Species-associated images in (B), (C), and (D) were reconstructed from the emission intensities of the PSII and two PSI components, respectively. (E) Ratio map of the PSI components with respect to the total emission signal. The ratio is indicated by the color scale. The ratio values were calculated only for pixels with signal intensities higher than a certain threshold, which was introduced to avoid divergent results due to divisions by tiny values. The scale bar indicates 10 μm. Panel F shows a histogram of the ratio values in (E). Panel G shows the representative spectra at positions 1 (BS) and 2 (M) indicated by the arrows in panel E.

cannot be regarded as SAS since they can be negative in some wavelength regions as shown in Fig. 2B. A search for physically meaningful SAS is generally model dependent [18,20]. To obtain SAS, here we conducted a global fitting of the basis spectra to linear combinations of three SAS candidates as,

$$\mathrm{SVD}_i(\nu) = \sum_{l=1}^{3} A_i^l SAS^l(\nu) \tag{1}$$

Here, $SAS^l(\nu)$ is the candidate for the l-th SAS, which for a mature *Z. mays* sample is expected to be assigned to a SAS related either to PSII or PSI. A_i^l is the relative amplitude of the l-th SAS in the i-th basis spectrum. While $SAS^l(\nu)$ should be positive over the whole spectral range, A^l can be either negative or positive. It has been known that the 77-K emission spectrum of the isolated PSII typically has three peaks at around 686 nm, 695 nm, and 730 nm [21–24]. Accordingly, we modeled each SAS as a sum of three skewed Gaussian functions [25] as

$$SAS^l(\nu) = \begin{cases} \sum_{m=1}^{3} F_m^l \exp\left(-\frac{1}{2}\cdot\left[\frac{1}{b_m^l}\ln\left(1+\frac{b_m^l(\nu-\nu_{0,m}^l)}{\Delta\nu_m^l}\right)\right]^2\right) & \left(1+\frac{b_m^l(\nu-\nu_{0,m}^l)}{\Delta\nu_m^l}>0\right) \\ 0 & \left(1+\frac{b_m^l(\nu-\nu_{0,m}^l)}{\Delta\nu_m^l}\le 0\right) \end{cases} \tag{2}$$

F_m^l, $\nu_{0,m}^l$, and $\Delta\nu_m^l$ are, respectively, the amplitude, peak wavenumber, and bandwidth of the m-th peak in the l-th SAS. The asymmetry parameter b_m^l makes the profile asymmetric. When it is negative/positive, the profile has a milder slope on the lower/higher energy side. When b_m^l equal 0, the profile converges to the Gaussian function. The fitting was conducted using the three basis spectra plotted against wavenumber ν. For the initial guess of the parameters, we referred to the known spectra of isolated PSI [26–28] and PSII [21–23] from higher plants. Global fitting was done with the constraint that the amplitude F_m^l becomes positive. Fig. 2C shows the SAS obtained from the global fitting outlined above. SAS shown in this article are normalized so that their spectral areas (integrated over wavenumber) give unity. As shown in the residual plot in Fig. 2A, there is no systematic deviation of the model functions from the basis spectra. The SAS assigned to PSII (dotted line in Fig. 2C) has two peaks at around 685 nm and 695 nm, and an additional broad peak at around 730 nm. Although the third peak might be assigned to the vibronic band of the main one, it seems to have an extraordinarily large amplitude as compared with the vibronic band of isolated PSII. This might be partly ascribed to the contamination of the PSI emission peak. We identified two SASs assigned to PSI: the two PSI components are tentatively named PSI-728 and PSI-735 after the peak wavelengths of the SASs at around 728 nm (dashed line in Fig. 2C) and at around 735 nm (solid line in Fig. 2C), respectively.

After the global fitting of the basis spectra, we fitted the 10,000 spectra contained in the 100 × 100-pixel fluorescence image to the linear combination of the three SASs. In this fitting, we fixed all of the parameters in Eq. 2 to the values predetermined by the global fitting of the basis spectra. A^l, the relative population of the l-th SAS component, was allowed to vary within the positive range. In Fig. S1, 100 randomly selected experimental spectra are compared with the model curves obtained by the fitting. Fig. S1 shows that, basically, the experimental spectra could be well fitted to the model curves except for slight deviations.

Fig. 1, panels B-D, shows images (hereafter called species-associated images) associated with the SASs of PSII and two PSI components. A species-associated image is obtained as a map of A^l. Since SASs in Eq. 1 are normalized so that their spectral areas integrated over wavenumber give unity, the species-associate image in this study is given as the spectral area of the species at a given pixel. It is clear that the image

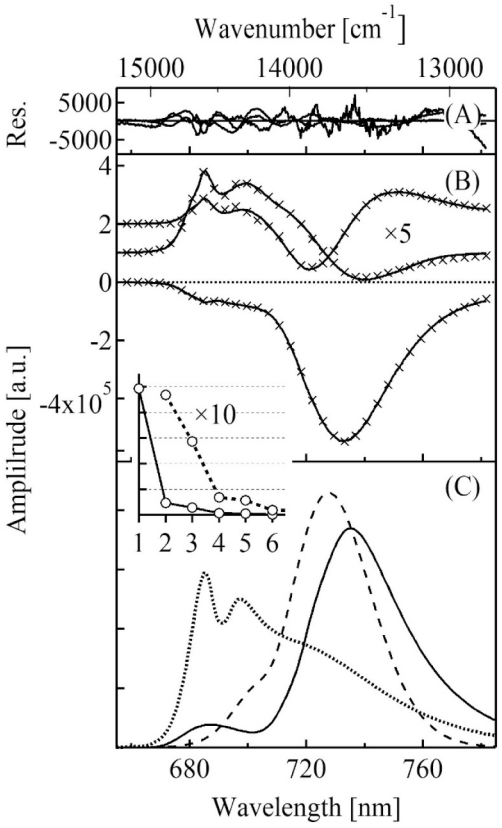

Fig. 2. Global fitting of the major basis spectra obtained from SVD analysis of the microscope data of a mature *Z. mays* leaf section at 80 K. (A) Residuals of the fitting curves from the basis spectra. (B) Three basis spectra (solid lines) and the fitting curves (crosses). The spectra are vertically offset to avoid overlap. The second and third basis spectra are magnified five times for easy comparison. (C) SAS expressed by the sum of three skewed Gaussian functions obtained by the global-fit iteration. The SASs shown by solid and dashed lines are assigned to PSI, and that indicated by a dotted line is assigned to PSII. The inset shows the six largest singular values, where the symbols connected by dotted line are ten-times magnified.

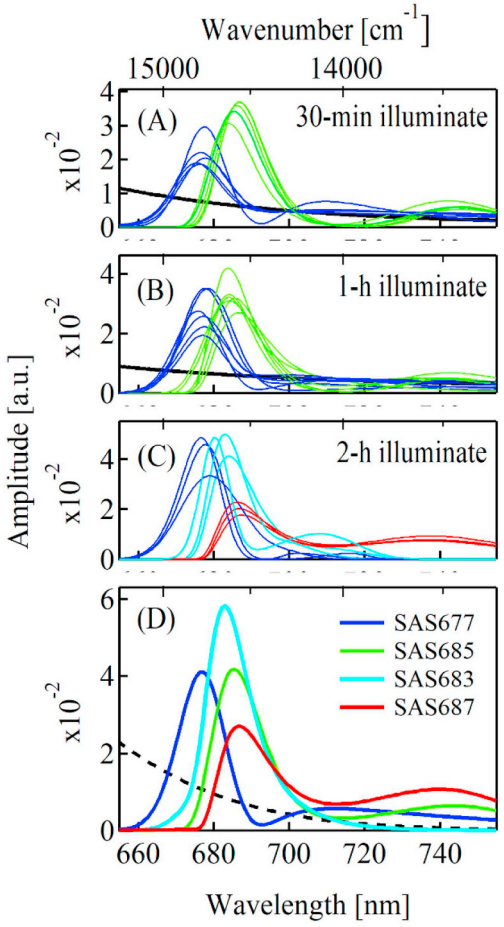

Fig. 3. Thin lines in panels A-C are SASs obtained from individual fluorescence images of leaf sections taken from plants illuminated for 30 min (A), 1 h (B), and 2 h (C). In panels A and B, additional SASs (black) were required for the satisfactory fitting of sloping baselines. Colored lines in panel D are SASs obtained from the global fitting using all basis spectra based on the four species model.

assigned to PSII has negligible intensities in cells around the vascular bundle, whereas those assigned to PSI have considerable intensities there. This becomes clearer in Fig. 1E, which shows a map of the relative PSI fluorescence intensity with respect to the total intensity. In BS cells, the ratio values almost reached unity, suggesting almost complete depletion of the PSII emission. The histogram of the ratio value shown in Fig. 1F indicates two clearly resolved peaks: one peak at unity is assigned to the BS cells, and the other, at around 0.7, is assigned to the M cells. Fig. 1G shows representative fluorescence spectra from an M cell (red) and a BS cell (blue) indicated by arrows in Fig. 1E. The PSII-specific emission peaks at around 685 nm and 695 nm are clearly seen in the spectrum from the M cell, while they are absent in that from the BS cell. In contrast to the sharp difference in the distributions of PSI and PSII, the two components assigned to PSI show similar spatial distributions with minor exceptions.

We conducted the same analysis as that described above for the results of etiolated *Z. mays* leaf sections illuminated for 30 min, 1 h, and 2 h. For samples illuminated for both 30 min and 1 h, the spectrum in any pixel of the images could be well reproduced by linear combination of the three basis spectra assigned to the first, second, and third largest SVs (see Fig. S2). From the global fit of the basis spectra, we could obtain three SASs as shown in Fig. 3A-B. Two of them (blue and green lines in Fig. 3) have peaks in the wavelength region of interest, while the other (black lines in Fig. 3) just gives a slope in the region and corresponds to the contribution from a broad emission band on the shorter wavelength side. The pigment giving the sloping SAS might be assigned to non-chlorophyllous pigments such as lignin, flavins, and so on. The contributions of these pigments might be observable because of the limited accumulation of photosynthetic pigments in this developmental stage.

Fig. 3 A-C shows SAS obtained for individual leaf sections. As shown in Fig. 3, a slightly different SAS was obtained for each individual leaf section. For leaves illuminated for 30 min and 1 h shown in panels A and B, respectively, two SASs have peaks at around 677 nm (blue) and 685 nm (green). Fig. 4 shows species-associated images for *Z. mays* leaf sections illuminated for 30 min (upper panels) and 1 h (lower panels). The fitting quality of the fluorescence spectrum at each pixel is shown in Fig. S3. For the section illuminated for 30 min, shown in Fig. 4A-C, SAS with the redder peak wavelength seems preferentially distributed in BS cells, as shown in a ratio map in Fig. 4C. However, this tendency was not always observed for other sections illuminated for 30 min. As will be discussed later, we found the opposite tendency for some other sections illuminated for 30 min (see Fig. S4 for example). For sections illuminated for 1 h, on the other hand, we repeatedly observed that SAS with the redder peak wavelength was preferentially distributed in BS cells as shown in a ratio map in Fig. 4H. Spectra in two representative positions in the ratio maps are compared in the right panels of Fig. 4.

For samples illuminated for 2 h, we again needed three SAS to satisfactorily reproduce the basis spectra (Fig. S5). In this case, all the three components have peaks in the wavelength region of interest. The

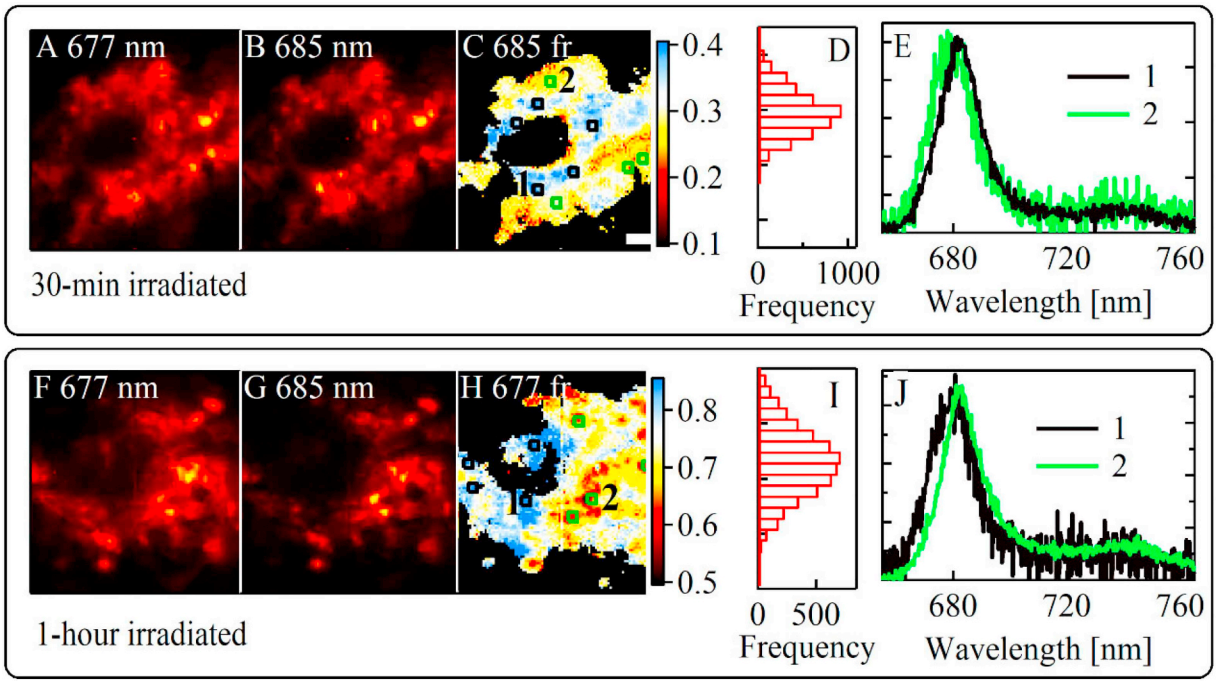

Fig. 4. Species-associated images around a vascular bundle of *Z. mays* leaf sections illuminated at room temperature for 30 min (A, B) and 1 h (F, G) and observed at 80 K. The images were reconstructed by the signal intensities of two species identified from the global fitting of the basis spectra (Fig. S2). The peak wavelengths of the species are indicated. (C) and (H) are ratio maps showing the relative intensities of the species shown in (B) and (F), respectively. The ratio is indicated by the color scale. The ratio values were calculated only for pixels with signal intensities higher than a certain threshold. The scale bar shows 10 μm. Panels (D) and (I) show histograms of the ratio values in (C) and (H), respectively. Curves in (E) and (J) are the fluorescence spectra at two representative locations indicated by the numbered squares in (C) and (H), respectively. The heights of the spectra are normalized for easy comparison.

sloping component needed in the fitting of 30-minute and 1-hour greening samples was not required, probably because a considerable accumulation of the chlorophyllous pigments hided its contribution after the 2-hour illumination. Forcing global fitting with two SAS components caused coalescence of the first and second SAS components and systematic deviations of the fitting curves, especially for the second basis spectrum (Fig. S5A). Fig. S6 shows the fitting of the fluorescence spectra in the image of the 2-hour-illuminated sample shown in Fig. 5 with the two SASs, which resulted in much larger deviations of the fitting curves than in the case including the third SAS (χ^2 values in the right panel of Fig. S6). The third SAS component has a rather intense side band at around 740 nm, which seems to be assigned to mature PSI. Fig. 5A-E shows the species-associated images and ratio maps for a leaf section illuminated for 2 h. As shown in Fig. 5E, the SAS at around 687 nm showed preferential localization in the region adjacent to VB, suggesting that it belongs to BS cells.

Fig. 5F shows fluorescence spectra at two representative locations assigned to BS (blue) and M (red) cells. The spectrum assigned to a BS cell showed a slightly higher intensity at around 740 nm and a slight red shift of the fluorescence peak at around 683 nm as compared with that assigned to an M cell. These facts reflect a larger concentration of the molecular species associated with the third SAS in the BS cell. In Fig. S7, we show a plot of the relative peak height of the 740-nm band vs. the 1st moment of the band at around 683 nm. The latter can be a rough measure of the peak wavelength of the band. Fig. S7 shows a slight positive correlation (correlation coefficient of 0.24) between these two quantities, manifesting a tendency that a pixel showing a red-shifted fluorescence peak has a higher intensity of the 740-nm band.

In Fig. 3A-C, we summarize the obtained SASs from the analysis of multiple individual leaf sections with the three different illumination conditions. All SASs shown in Fig. 3 were normalized so that their spectral areas become unity. There are certain degrees of individual variations in the spectral profiles of SASs among leaf sections with the same illumination condition except for the sloping baseline component shown in black. We needed at least three SAS components to obtain satisfactory fitting quality for the samples illuminated for 2 h. Among the three components for the samples illuminated for 2 h, the one peaking at around 677 nm was common to all illumination conditions investigated. On the other hand, the other two components with peaks at around 683 nm (cyan) and 687 nm (red) were different from that with a peak at around 685 nm (green) observed in the samples illuminated for 30 min and 1 h. Thus, the present study suggested that we need at least 4 types of SASs for *Z. mays* leaf sections greening under illumination of up to 2 h.

According to the observations summarized above, we next analyzed the full set of the obtained spectral data based on a model assuming five SAS components. In this model, any fluorescence spectrum in the whole data set is fitted to a linear combination of the five predetermined SASs that are common to every illumination condition. Since one of the five SASs expresses just the sloping baseline, hereafter, we call this model the 4-SAS model. To obtain the SASs, we conducted global fitting of all the obtained basis spectra associated with significantly large singular values. As shown in Fig. S8, all of the basis spectra could be well reproduced by linear combinations of the five SAS components given by Eq. (2). As shown in Fig. 3D, the five SAS components thus obtained have peak wavelengths similar to those obtained from the analyses of the individual leaf sections shown in Fig. 3A-C. Peak wavelengths ν_0, widths $\Delta\nu$, and b parameters of the main bands of the four SAS component are summarized in Table 1. For the full list of the parameters, see Table S1 in supporting information. We named the components SAS677, SAS685, SAS683, and SAS687 after their peak wavelengths. We again fitted the fluorescence spectra at every pixel in the images to the linear combination of the five SASs shown in Fig. 3D. The fitting quality with the 4-SAS model was comparable to that obtained with the independent fitting of individual leaf sections.

Now, all of the fluorescence images obtained by the present study were decomposed into the contributions of four SAS components. As shown in Fig. 6 top panel, we calculated the fraction of each SAS signal

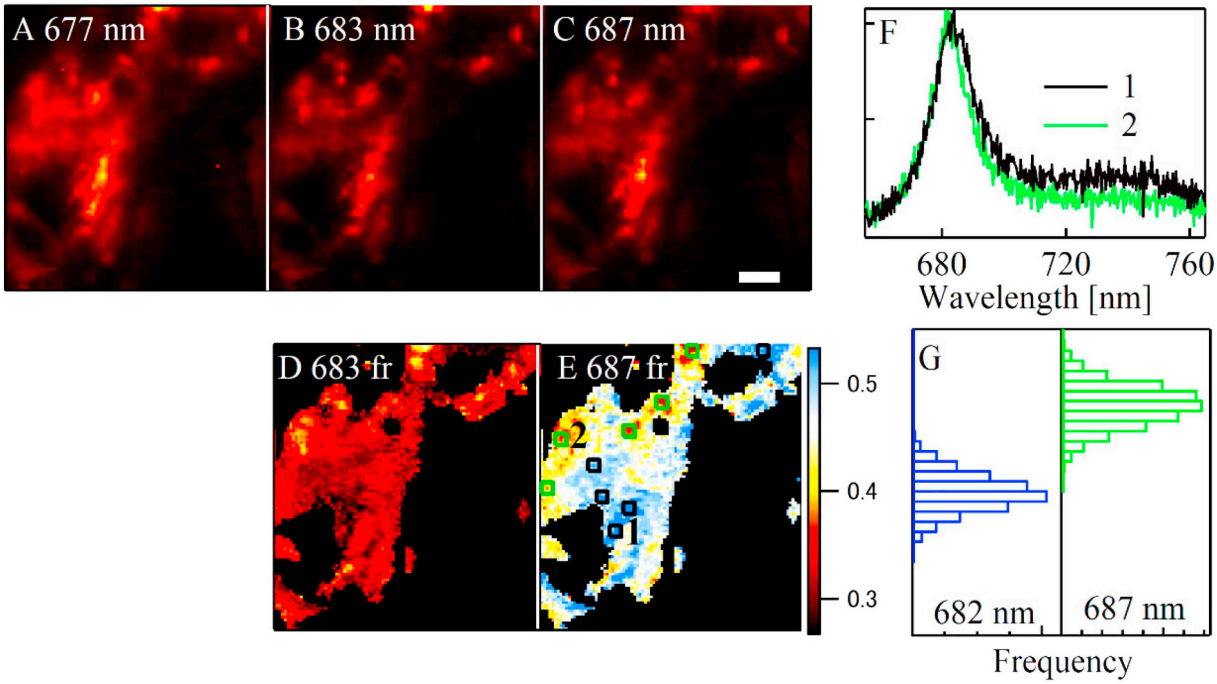

Fig. 5. Species-associated images (A-C) around two vascular bundles of a *Z. mays* leaf section illuminated at room temperature for ca. 2 h and observed at 80 K. The peak wavelengths of the species are indicated. (D) and (E) are ratio maps showing the relative intensities of the species shown in (B) and (C), respectively. The ratio is indicated with the color scale. The ratio values were calculated only for pixels with signal intensities higher than a certain threshold. The scale bar shows 10 μm. Curves in (F) are the fluorescence spectra at two representative locations indicated by the numbered squares in (E). The heights of the spectra are normalized for easy comparison. Panel G shows histograms of the ratio values in (D) (blue) and (E) (green). (For interpretation of the references to color in this figure legend, the reader is referred to the web version of this article.)

Table 1
The peak wavelength, width, and *b*-parameters of SAS components.

	peak [nm]	width [cm^{-1}]	*b*
SAS677	676.9 ± 0.05	132 ± 1.2	0.077 ± 0.008
SAS685	685.4 ± 0.04	137 ± 0.6	−0.266 ± 0.006
SAS683	682.8 ± 0.20	106 ± 4.0	−0.250 ± 0.032
SAS687	686.7 ± 0.44	138 ± 5.0	−0.452 ± 0.055

in an image to obtain its temporal evolution. The error bars indicate the standard deviations of multiple leaf-section data. We could visualize the buildup of SAS683 and SAS687, in contrast to the rapid decrease of SAS685 during greening. The fraction of SAS677 did not change significantly.

To evaluate the preferential localization of each SAS component in BS or M cells under the greening process, we next calculated the fraction of each SAS signal with respect to the total fluorescence signal within typical BS and M cells. We selected several leaf-section images showing (a) clear VB structure(s). From each ratio map of the selected image, we picked up several areas that can be assigned to BS and M cells. There is a certain amount of heterogeneity in the SAS fraction within cells located near or far from the VB. For example in the ratio map in Fig. 4C, although the region near the VB tended to show a higher fraction of SAS685, several other regions showed relatively low SAS685 fractions. This may reflect the heterogeneous development of cell differentiation. In this particular case, we designated areas with high SAS685 fractions as typical BS cells, whereas we excluded those with low SAS685 fractions from typical BS cells. The boxes drawn by the black and green lines in Figs. 4C, H, and 5E show examples of such areas assigned to BS and M cells, respectively. Each box is composed of 4 × 4 = 16 pixels. 10 to 17 areas were selected as typical BS or M cell regions from three independent leaf sections for each illumination condition.

Fig. 6, lower panel, shows the fraction thus calculated of each SAS component in regions assigned to M (left) and BS (right) cells. Error bars show the estimated standard deviations. Asterisks are given over the bars for which significant differences between M and BS cells were demonstrated based on the Welch's *t*-test with a 5% significance level. The ratio map in Fig. 4C gave an impression that SAS685 is preferentially localized in BS cells in the sample illuminated for 30 min. However, this view is not supported by the statistical analysis (see also Fig. S4). Large standard deviations for the fractions of SAS677 and SAS685 for the sample illuminated for 30 min indicate the heterogeneous nature of the fluorescence properties in leaves at this greening stage. SAS683 was found to be significantly enhanced in M cells for leaves illuminated for both 1 and 2 h. We will not focus much on the opposite tendency of SAS683 to be enhanced in BS cells for the leaves illuminated for 30 min, since the accumulation of this SAS component is negligible in this greening stage. According to the results shown in Fig. 6 lower panel, we can designate SAS683 as a potential PSII precursor. The large side band at around 740 nm of SAS687 suggests its relevance to PSI. The enhanced accumulation of SAS687 in BS cells in leaves illuminated for 2 h also favors this assignment.

4. Discussion

4.1. Microscope observations of photosystem localizations in mature Zea mays

The present cryogenic microscope observation succeeded in visualizing the different localizations of PSs in BS and M cells of mature *Z. mays* leaf sections. The present study is not the first to succeed in the optical microscope observations of different localizations of PSs in a C4 plant [10,29–31]. Nevertheless, measuring at 80 K could drastically improve the spectral resolution between the two PSs, giving clearly resolved differentiated localizations of them (Fig. 1). Three SAS components could be deduced from the spectral decomposition with the aid of SVD analysis. Two of the three were assigned to PSI and the other to PSII.

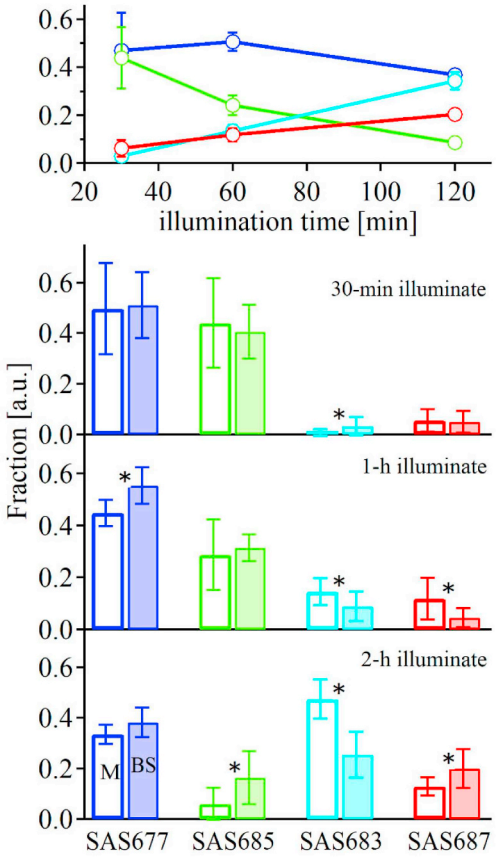

Fig. 6. (Top) Illumination-induced time evolution of the fractions of SAS677 (blue), SAS685 (green), SAS683 (cyan), and SAS687 (red) with respect to the total fluorescence signals over the total area of images. The error bars indicate the standard deviations. The bars in the lower panel show the fractions of the species averaged over multiple areas of 4 × 4 pixels selected as typical M (left) or BS (right) cells. The error bars indicate standard deviations over 13 (M and BS cells illuminated for 30 min), 17 (M illuminated for 1 h), 14 (BS illuminated for 1 h), and 10 (M and BS illuminated for 2 h) areas selected. Asterisks indicate bars for which significant differences were demonstrated between the M and BS cells based on the Welch's *t*-test ($p < .05$). (For interpretation of the references to color in this figure legend, the reader is referred to the web version of this article.)

The two SASs for PSI have peaks at around 728 nm and 735 nm (Fig. 2C). Wientjes et al. revealed that both the PSI core and LHCI of higher plants contain red Chls responsible for the specific red-shifted emission peak at 77 K [26,27]. Their study showed that the peak position of the 77-K emission is at around 721 nm for the PSI core, whereas it shifts to 733 nm upon the full assembly of the PSI-LHCI super-complex. The SAS with a peak at around 735 nm might be assigned to the emission spectrum of the in vivo PSI-LHCI super-complex. The 3-nm red shift from that of the isolated PSI-LHCI might be due to contamination of vibronic bands. On the other hand, the other SAS has its peak at 728 nm, between those of the PSI core and PSI-LHCI, and is too red shifted to be assigned to the PSI core. Here we tentatively assign this SAS component to the PSI-LHCI super-complex with a reduced emission quantum yield of the reddest Chl in LHCI. In Fig. 1G, the blue curve for a BS cell shows a red-shifted PSI band as compared with that of the red curve (M cell), suggesting an enhanced population of the 735-nm component. Thus, the present result suggests different compositions of LHCI between M and BS cells.

The ratio map in Fig. 1E indicates that the PSII emission is almost completely suppressed in BS cells. The histogram shown in Fig. 1F indicates that the PSI emission intensity dominates about 70% of the total emission in M cells, while it is exclusive in BS cells. This seems to contradict the current knowledge about the PSII content in BS cells of *Z. mays*: several proteomic and transcriptomic studies have suggested that a small amount of PSII components remains in BS cells of *Z. mays*, although its content is drastically reduced [32,33]. Quantitative analysis showed that the PSII content in BS cells is reduced to ca. 20% of that in M cells, while the PSI content is ca. 40% enhanced in BS cells [32]. These conclusions were roughly supported by previous studies using fluorescence lifetime imaging (FLIM) on C4 plants at room temperature [29,31]. These values give a rough estimation that the ratio of ca. 7:3 of the PSI:PSII emission in M cells obtained in the present study will increase to $7 \times 1.4{:}3 \times 0.2 \approx 94{:}6$ in BS cells. Thus, the above estimation predicts that the PSII emission contributes to about 6% of the total intensity in BS cells, which should be above the detection limit of the present measurements.

We can consider several possible reasons for the apparent contradiction between the present observation and the previous proteomic studies with respect to the amount of PSII in BS cells. The previous studies indicated that the level of LHCII is not reduced much in BS cells, in contrast to the drastic reduction of the proteins composing the PSII core complex. LHCII remaining in BS cells might partly play a function in harvesting light energy for PSI. Thus, the lower PSII emission in BS cells than expected can be explained by the enhanced emission from PSI due to its assembling with the functional LHCII. A native PAGE experiment done by Majeran et al. suggested that in BS cells the dimeric PSII super-complex was not detected, whereas monomeric or partially formed super-complexes were detected [32]. Thus, at least some of the PSII subunits in BS cells detected in proteomic studies are not fully assembled, resulting in the further reduction of the specific fluorescence emission.

4.2. Four spectral components identified in greening Zea mays

In the present study, we identified four spectral components named SAS677, SAS685, SAS683, and SAS687 by using the SVD-based fitting analysis. Here we assumed SAS profiles composed of two bands; the first peak at the shorter wavelength side is interpreted as the 0–0 band, and the second one on the longer wavelength side is attributed either to vibronic origin or to mature PSI-specific red Chl emission. Since the vibronic band generally has a small contribution, the estimations of their peak positions and relative intensities are less reliable. This is not true exceptionally for SAS687, since it has a relatively large second band at around 740 nm. The red-shifted first band of SAS687 and its relatively large second band are consistent with the observation in Fig. 5. As shown in Fig. 5, we observed the correlation between the red shift of the main band and the increase of the sub-band at around 740 nm in the samples illuminated for 2 h (Fig. S7). This observation predicts the existence of a spectral component with a red-shifted first band and a relatively large second band at around 740 nm. SAS687 has the characteristics expected from this observation.

Among four SAS components, SAS683 and SAS687 show a trend of gradual accumulation during prolonged illumination. On the other hand, the other two components have dominant populations in the 30-min illumination phase, while their fractions slightly (for SAS677) or drastically (for SAS685) decrease upon further illumination. In our previous study [10], we revealed large variability in the peak positions and widths of the fluorescence spectra, especially for *Z. mays* leaf sections illuminated for 1 h [10]. The study of Shibata et al. [10] used the same illumination intensity and spectrum for the greening as those used here. That study showed that for samples illuminated for 1 h there was a tendency for fluorescence spectra with blue-shifted peaks (around 679 nm) to have broader spectral widths than those with red-shifted peaks (around 682 nm). The present study basically reproduced this observation as shown in Fig. 4J. The present analysis suggested that the broader widths of blue-shifted emission spectra are due to the larger contribution from SAS677. The previous study also revealed that in samples illuminated for 3 h, a fluorescence band at around 730 nm

became conspicuous in BS cells, suggesting the accumulation of mature PSI. These previous observations are in line with the present results that show increased SAS687 after 2 h of illumination.

Basically, we can assign SAS components with a larger fraction in BS and M cells to potential precursors to PSI and PSII, respectively. Marchand et al. reported that BS and M cells of *Z. mays* show distinct characteristics of fluorescence spectra at 77 K, even in etiolated leaves [9]. On the other hand, an early study by Shuster et al. has suggested the poor differentiation of chloroplasts of *Z. mays* within ca. 4-hour greening by light illumination [6]. In fact, in the present study the greening leaf sections showed only poor differentiated localizations of the SAS components (see single-peaked histograms in Figs. 4D, I and 5G) in contrast to the well-differentiated PS distributions in mature *Z mays* leaves (see double-peaked histogram in Fig. 1F). The poor differentiation is considered to be partly due to the fact that each SAS component is contributed by multiple species accumulating in the sample. Nonetheless, we could find a preferential localization of SAS683 in the M cells, as shown in Fig. 6. Thus, we are confident in designating SAS683 as a PSII precursor. The gradual accumulation of SAS683 (Fig. 6) also favors this assignment. Since SAS687 has a large 740-nm sub-band specific to the mature PSI, it is reasonable to assign this component to the potential PSI precursor. This interpretation is supported by its preferential localization in BS cells in the sample illuminated for 2 h.

4.3. SAS677 is the final product of Chl synthesis

From the above criterion, SAS677 might be designated as a precursor to PSI in principle since it has an enhanced localization in BS cells of samples irradiated for 1 h (Figs. 4H and 6). However, several reports have shown that light-transformed chlorophyllide remaining bound to POR will show fluorescence bands at around 675–680 nm after the disassociation from the self-aggregates composed of the protochlorophyllide-binding POR in prolamellar bodies [34,35]. Chl just after the esterification is also responsible for the short-wavelength emission. In fact, Fig. 6 top panel shows that SAS677 is a dominant component after 30-min and 60-min illumination while its fraction slightly decreases with further prolonged illumination. Thus, we concluded here that SAS677 is due to the product of the final stage of Chl synthesis, which is not assembled into photosynthetic proteins.

4.4. Intermediates relevant to PSs

The current model of PSI and PSII assembly assumes a stepwise buildup of these super-complexes. For the PSII assembly [11–13], it has been proposed that the process begins with the formation of the reaction center (D1-D2-cyt559), followed by the bindings of the CP47 part and then of the CP43 part. The oxygen-evolving complex is assembled in the later stage, and the dimerization of the complex finalizes the process. The sequential assembly has also been proposed for PSI [14–16]. The model assumes that pre-existing PsaB dimerizes with PsaA to form the core hetero dimer in the first step, and then peripheral subunits are integrated. Many auxiliary factors for the assemblies of photosynthetic super-complexes have been identified [13,36].

As discussed above, SAS683 can be designated as a precursor relevant to PSII. The stepwise model of the PSII assembly suggests that M cells under greening accumulate PSII-relevant assembly intermediates, i.e., RC (682 nm [37]), RC-CP47 (694 nm [38]), CP47 free from RC (690 nm [39]), and CP43 free from RC (685 nm [40]). The numbers in the parentheses are the peak wavelengths of the 77-K fluorescence spectra of analogous complexes isolated from mature PSII found in the literature. If we focus only on the similarity of the fluorescence peak wavelengths, SAS683 is attributable to the RC complex of PSII. This assignment is also compatible with the early studies by Ohashi et al. [41,42], suggesting that the photochemical activity of PSII appears after 1–1.5 h of illumination to etiolated barley. If this is the case, the M cells of etiolated *Z. mays* accumulate mainly RC of PSII after the 2-hour greening.

Of course, we must consider the possibility that the spectral profiles of assembly intermediates listed above are significantly different from those of their analogous complexes isolated from the mature PSII. Assembly intermediates form super-complexes with several auxiliary proteins [43], which may show vastly different spectral properties. On the other hand, co-translational pigment insertion has been a prevailing model [44]. It is hypothesized that the synthesis of Chl and its insertion into newly synthesized PS polypeptides are coordinated in the metabolon, a hypothetical large protein complex composed of enzymes catalyzing the Chl synthesis, the ribosome responsible for the polypeptide synthesis, and other auxiliary proteins involved in the assembly process [45,46]. SAS683 may correspond to a large super-complex, such as the metabolon.

SAS687 showed enhanced localization in BS cells (Figs. 5 and 6), indicating its relevance to PSI. The strong sub-band at around 740 nm is roughly consistent with the 77-K fluorescence spectrum of the mature PSI, thus supporting this assignment. SAS687 probably originates from a mixture of the PSI intermediate species with its mature form. An early study by Schuster et al. reported a fluorescence spectrum at around 686 nm, similar to that of SAS687, from BS cells isolated from etiolated *Z. mays* illuminated for 8 h [6]. In their study, further illumination for 24 h induced the PSI-specific 77-K fluorescence band at around 730 nm. They interpreted the species emitting at around 686 nm due to PSI which has not yet fully organized. It is unfortunately not clear whether the illumination condition to the etiolated leaf in their study was similar to that in the present study. Nevertheless, the similarity in the peak wavelengths of the fluorescent species reported by Shuster et al. and SAS687 detected here suggests their relevance. The species emitting the band at around 687 nm pre-exists before the accumulation of the mature PSI. If we again assume the *co*-translational pigment insertion to the newly synthesized PSI polypeptides, the species associated with the 687-nm emission can be assigned to the complex functioning as the pigment pool to supply the cofactors to the newly synthesized protein.

It has been revealed that the peripheral antenna and their cofactor pigment Chl-*b* accumulate subsequent to the development of the core complexes of PSs [41,47]. On the other hand, the peak wavelength of the sub-band of SAS687 was observed at around 740 nm, which can be assigned to the red Chls in LHCI rather than to those in the PSI core complex [26,27]. Although we cannot exclude the possible contamination of the vibronic bands of other components to the sub-band, the long-wavelength sub-band of SAS687 might suggest the assembly of a PSI-LHCI super-complex.

5. Concluding remarks

The present study demonstrates that cryogenic fluorescence microspectroscopy is effective in distinguishing differentiated cells in C4 plant leaves. We could observe clearly differentiated PS distributions in the mature *Z. mays* leaf sections. For the 30-min greening *Z. mays* leaves, the fluorescence spectral properties of cells showed no clear trend of differentiation. From the aid of the SVD analysis, we could identify four components, SAS677, SAS685, SAS683, and SAS687, in greening *Z. mays* leaves. The 1–2-hour irradiation to etiolated *Z. mays* eventually resulted in different accumulations of SAS683 and SAS687 between cells adjacent and far from the VB. SAS677 was designated as chlorophyllide or Chl just synthesized and before insertion into the photosynthetic proteins. SAS683 is a precursor to PSII, possibly assigned to PSII RC. SAS687 was assigned to the PSI precursor. The sub-band of this component at around 740 nm indicates the partial formation of red Chl specific for PSI.

Transparency document

The Transparency document associated with this article can be found, in online version

Acknowledgments

This work was financially supported in part by Yamada Science Foundation and by JSPS KAKENHI Grant Numbers JP24370060, JP26650043, and JP15H04356 to Y.S.

Appendix A. Supplementary data

Supplementary data to this article can be found online at https://doi.org/10.1016/j.bbabio.2019.148090.

References

[1] Y. Umena, K. Kawakami, J.R. Shen, N. Kamiya, Crystal structure of oxygen-evolving photosystem II at a resolution of 19 angstrom, Nature 473 (2011) 55–60.
[2] X.C. Qin, M. Suga, T.Y. Kuang, J.R. Shen, Structural basis for energy transfer pathways in the plant PSI-LHCI supercomplex, Science 348 (2015) 989–995.
[3] X.P. Wei, X.D. Su, P. Cao, X.Y. Liu, W.R. Chang, M. Li, X.Z. Zhang, Z.F. Liu, Structure of spinach photosystem II-LHCII supercomplex at 3.2 angstrom resolution, Nature 534 (2016) 69–74.
[4] K. Shibata, Spectroscopic studies on chlorophyll formation in intact leaves, J. Biochem. 44 (1957) 147–173.
[5] W.L. Butler, W.R. Briggs, Relation between structure and pigments during first stages of proplastid greening, Biochim. Biophys. Acta 112 (1966) 45–53.
[6] G. Schuster, I. Ohad, B. Martineau, W.C. Taylor, Differentiation and development of bundle sheath and mesophyll thylakoids in maize - thylakoid polypeptide composition, phosphorylation, and organization of photosystem-II, J. Biol. Chem. 260 (1985) 1866–1873.
[7] F. Franck, P. Eullaffroy, R. Popovic, Formation of long-wavelength chlorophyllide (Chlide695) is required for the assembly of photosystem II in etiolated barley leaves, Photosynth. Res. 51 (1997) 107–118.
[8] C. Sundqvist, C. Dahlin, With chlorophyll pigments from prolamellar bodies to light-harvesting complexes, Physiol. Plantarum 100 (1997) 748–759.
[9] M. Marchand, D. Dewez, F. Franck, R. Popovic, Protochlorophyllide photo-transformation in the bundle sheath cells of *Zea mays*, J. Photochem. Photobiol. B 75 (2004) 73–80.
[10] Y. Shibata, W. Katoh, Y. Tahara, Study of cell-differentiation and assembly of photosynthetic proteins during greening of etiolated *Zea mays* leaves using confocal fluorescence microspectroscopy at liquid-nitrogen temperature, Biochim. Biophys. Acta Bioenerg. 1827 (2013) 520–528.
[11] J. Komenda, V. Reisinger, B.C. Müller, M. Dobáková, B. Granvogl, L.A. Eichacker, Accumulation of the D2 protein is a key regulatory step for assembly of the photosystem II reaction center complex in *Synechocystis* PCC 6803, J. Biol. Chem. 279 (2004) 48620–48629.
[12] P.J. Nixon, F. Michoux, J.F. Yu, M. Boehm, J. Komenda, Recent advances in understanding the assembly and repair of photosystem II, Ann. Bot.-London 106 (2010) 1–16.
[13] J. Nickelsen, B. Rengstl, Photosystem II assembly: from cyanobacteria to plants, Annu. Rev. Plant Biol. 64 (2013) 609–635.
[14] S. Ozawa, J. Nield, A. Terao, E.J. Stauber, M. Hippler, H. Koike, J.D. Rochaix, Y. Takahashi, Biochemical and structural studies of the large Ycf4-photosystem I assembly complex of the green alga *Chlamydomonas reinhardtii*, Plant Cell 21 (2009) 2424–2442.
[15] S. Ozawa, T. Onishi, Y. Takahashi, Identification and characterization of an assembly intermediate subcomplex of photosystem I in the green alga *Chlamydomonas reinhardtii*, J. Biol. Chem. 285 (2010) 20072–20079.
[16] S. Nellaepalli, S.I. Ozawal, H. Kuroda, Y. Takahashi, The photosystem I assembly apparatus consisting of Ycf3-Y3IP1 and Ycf4 modules, Nat. Commun. 9 (2018).
[17] Y. Shibata, W. Katoh, T. Chiba, K. Namie, N. Ohnishi, J. Minagawa, H. Nakanishi, T. Noguchi, H. Fukumura, Development of a novel cryogenic microscope with numerical aperture of 0.9 and its application to photosynthesis research, Biochim. Biophys. Acta Bioenerg. 1837 (2014) 880–887.
[18] J. Hofrichter, J.H. Sommer, E.R. Henry, W.A. Eaton, Nanosecond absorption-spectroscopy of hemoglobin - elementary processes in kinetic cooperativity, Proc. Natl. Acad. Sci. 80 (1983) 2235–2239.
[19] S. Kumazaki, M. Akari, M. Hasegawa, Transformation of thylakoid membranes during differentiation from vegetative cell into heterocyst visualized by microscopic spectral imaging, Plant Physiol. 161 (2013) 1321–1333.
[20] R.I. Shrager, R.W. Hendler, Titration of individual components in a mixture with resolution of difference spectra, pKs, and redox transitions, Anal. Chem. 54 (1982) 1147–1152.
[21] R.J. van Dorssen, J.J. Plijter, J.P. Dekker, A. den Ouden, J. Amesz, H.J. van Gorkom, Spectroscopic properties of chloroplast grana membranes and of the core of photosystem-II, Biochim. Biophys. Acta 890 (1987) 134–143.
[22] M. Alfonso, G. Montoya, R. Cases, R. Rodríguez, R. Picorel, Core antenna complexes, CP43 and CP47, of higher-plant photosystem-II - spectral properties, pigment stoichiometry, and amino-acid-composition, Biochemistry 33 (1994) 10494–10500.
[23] A. Mohamed, R. Nagao, T. Noguchi, H. Fukumura, Y. Shibata, Structure-based modeling of fluorescence kinetics of photosystem II: relation between its dimeric form and photoregulation, J. Phys. Chem. B 120 (2016) 365–376.
[24] J.J. Lamb, G. Røkke, M.F. Hohmann-Marriott, Chlorophyll fluorescence emission spectroscopy of oxygenic organisms at 77 K, Photosynthetica 56 (2018) 105–124.
[25] J.M. Sevilla, M. Dominguez, F. Garcia-Blanco, M. Blazquez, Resolution of absorption-spectra, Comput. Chem. 13 (1989) 197–200.
[26] E. Wientjes, R. Croce, The light-harvesting complexes of higher-plant photosystem I: Lhca1/4 and Lhca2/3 form two red-emitting heterodimers, Biochem. J. 433 (2011) 477–485.
[27] E. Wientjes, I.H.M. van Stokkum, H. van Amerongen, R. Croce, The role of the individual Lhcas in photosystem I excitation energy trapping, Biophys. J. 101 (2011) 745–754.
[28] R. Croce, H. van Amerongen, Light-harvesting in photosystem I, Photosynth. Res. 116 (2013) 153–166.
[29] M. Hasegawa, T. Shiina, M. Terazima, S. Kumazaki, Selective excitation of photosystems in chloroplasts inside plant leaves observed by near-infrared laser-based fluorescence spectral microscopy, Plant Cell Physiol. 51 (2010) 225–238.
[30] M. Hasegawa, T. Yoshida, M. Yabuta, M. Terazima, S. Kumazaki, Anti-stokes fluorescence spectra of chloroplasts in *Parachlorella kessleri* and maize at room temperature as characterized by near-infrared continuous-wave laser fluorescence microscopy and absorption microscopy, J. Phys. Chem. B 115 (2011) 4184–4194.
[31] I. Iermak, J. Vink, A.N. Bader, E. Wientjes, H. van Amerongen, Visualizing heterogeneity of photosynthetic properties of plant leaves with two-photon fluorescence lifetime imaging microscopy, Biochim. Biophys. Acta Bioenerg. 1857 (2016) 1473–1478.
[32] W. Majeran, B. Zybailov, A.J. Ytterberg, J. Dunsmore, Q. Sun, K.J. van Wijk, Consequences of C-4 differentiation for chloroplast membrane proteomes in maize mesophyll and bundle sheath cells, Mol. Cell. Proteomics 7 (2008) 1609–1638.
[33] R.M. Sharpe, A. Mahajan, E.M. Takacs, D.B. Stern, A.B. Cahoon, Developmental and cell type characterization of bundle sheath and mesophyll chloroplast transcript abundance in maize, Curr. Genet. 57 (2011) 89–102.
[34] B. Schoefs, Protochlorophyllide reduction - what is new in 2005? Photosynthetica 43 (2005) 329–343.
[35] D. Kovacevic, D. Dewez, R. Popovic, Irradiation-induced in vivo re-localization of NADPH-protochlorophyllide oxidoreductase from prolamellar body to stroma of barley etioplast, Photosynthetica 45 (2007) 105–109.
[36] H.X. Yang, J. Liu, X.G. Wen, C.M. Lu, Molecular mechanism of photosystem I assembly in oxygenic organisms, Biochim. Biophys. Acta Bioenerg. 1847 (2015) 838–848.
[37] M.L. Groot, E.J. Peterman, P.J. van Kan, I.H. van Stokkum, J.P. Dekker, R. van Grondelle, Temperature-dependent triplet and fluorescence quantum yields of the photosystem-II reaction-center described in a thermodynamic model, Biophys. J. 67 (1994) 318–330.
[38] E.G. Andrizhiyevskaya, A. Chojnicka, J.A. Bautista, B.A. Diner, R. van Grondelle, J.P. Dekker, Origin of the F685 and F695 fluorescence in photosystem II, Photosynth. Res. 84 (2005) 173–180.
[39] M.L. Groot, E.J.G. Peterman, I.H.M. van Stokkum, J.P. Dekker, R. van Grondelle, Triplet and fluorescing states of the CP47 antenna complex of photosystem-II studied as a function of temperature, Biophys. J. 68 (1995) 281–290.
[40] M.L. Groot, R.N. Frese, F.L. de Weerd, K. Bromek, A. Pettersson, E.J.G. Peterman, I.H.M. van Stokkum, R. van Grondelle, J.P. Dekker, Spectroscopic properties of the CP43 core antenna protein of photosystem II, Biophys. J. 77 (1999) 3328–3340.
[41] K. Ohashi, A. Tanaka, H. Tsuji, Formation of the photosynthetic electron-transport system during the early phase of greening in barley leaves, Plant Physiol. 91 (1989) 409–414.
[42] K. Ohashi, A. Murakami, A. Tanaka, H. Tsuji, Y. Fujita, Developmental-changes in amounts of thylakoid components in plastids of barley leaves, Plant Cell Physiol. 33 (1992) 371–377.
[43] Y. Lu, Identification and roles of photosystem II assembly, stability and repair factors in *Arabidopsis*, Front. Plant Sci. 7 (2016).
[44] P. Wang, B. Grimm, Organization of chlorophyll biosynthesis and insertion of chlorophyll into the chlorophyll-binding proteins in chloroplasts, Photosynth. Res. 126 (2015) 189–202.
[45] B.S.J. Winkel, Metabolic channeling in plants, Annu. Rev. Plant Biol. 55 (2004) 85–107.
[46] K. Jørgensen, A.V. Rasmussen, M. Morant, A.H. Nielsen, N. Bjarnholt, M. Zagrobelny, S. Bak, B.L. Møller, Metabolon formation and metabolic channeling in the biosynthesis of plant natural products, Curr. Opin. Plant Biol. 8 (2005) 280–291.
[47] E. Kanervo, M. Singh, M. Suorsa, V. Paakkarinen, E. Aro, N. Battchikova, E.M. Aro, Expression of protein complexes and individual proteins upon transition of etioplasts to chloroplasts in pea (Pisum sativum), Plant Cell Physiol. 49 (2008) 396–410.